Bioluminescent imaging identifies thymus, as overlooked colonized organ, in a chronic model *of Leishmania donovani* mouse visceral leishmaniasis

Bárbara Domínguez-Asenjo[1], Camino Gutiérrez-Corbo[1], Yolanda Pérez-Pertejo[1], Salvador Iborra[2], Rafael Balaña-Fouce[1*], Rosa Mª Reguera Torres[1*]

[1]Department of Biomedical Sciences, Faculty of Veterinary Medicine, University of León, 24071 León, Spain.

[2]Department of Immunology, Ophthalmology and ENT. Complutense University School of Medicine and 12 de Octubre Health Research Institute (imas12), 28040 Madrid, Spain.

***** Corresponding authors

Abbreviations: Visceral leishmaniasis (VL); cyclophosphamide (CPP); Miltefosine 40 mg/kg/day (M40); Miltefosine 10 mg/kg/day (M10); Drugs for neglected diseases initiative (DNDi); weeks post-infection (wpi); quantitative PCR (qPCR); ribosomal RNA(rRNA); kinetoplastid DNA (kDNA); regions of interest (RoI); fetal bovine serum (FBS).

Keyworks: *Leishmania donovani, drug discovery, in vivo imaging, thymus*

Abstract

The search for new drugs against neglected parasitic diseases has experienced a major boost in recent years with the incorporation of bioimaging techniques. Visceral leishmaniasis, the second more neglected disease in the world, has effective treatments, but with several disadvantages that make the search for new therapeutic solutions an urgent task. Animal models of visceral leishmaniasis that resemble the human disease have the disadvantage of using hamsters, which is an outbred breeding animal too large to obtain acceptable images with current bioimaging methodologies. Mouse models of visceral leishmaniasis seem, however, to be more suitable for early (acute) stages of the disease, but not for chronic ones. In our work, we describe a chronic Balb/c mouse model in which the infection primarily colonizes the spleen and well recreates the late stages of human disease. Thanks to the bioluminescent image, we have been able to identify experimentally, for the first time, a new primary lymphoid organ of colonization, the thymus, which appears infected from the beginning until the late phases of the infection, and which can be a reservoir of possible relapses after treatment with miltefosine, the oral antileishmanial drug used in clinical practice.

Introduction

Visceral leishmaniasis (VL) is a zoonotic neglected disease produced by single-celled parasites of the genus *Leishmania* (*Leishmania infantum* and *Leishmania donovani*) and transmitted by *Phlebotomus* and *Lutzomya* sandflies[1]. *L. donovani* is mainly transmitted from human to human, unlike *L. infantum*, whose transmission is mostly zoonotic. Although VL is a disease known for centuries and has a high mortality (according to WHO, the incidence is of more than 30,000 fatalities per year in the absence of treatment (https://www.who.int/health-topics/leishmaniasis#tab=tab_1)), no effective vaccine for humans is yet available. In addition, the existing drugs are unsafe, ineffective in certain geographical areas due to the emergence of resistance, and mostly depend on parenteral administration, which reduce patient adherence to long periods of treatment [2,3].

The high prevalence of these diseases in endemic regions of the planet, the suffering caused by the disease, not only from a health perspective but also from an economic point of view, and the lack of general interest in the so-called neglected diseases, make research into safer and more effective therapeutic alternatives by all public and private stakeholders more necessary than ever in order to eradicate them in the shortest time possible[2].

The research of new drugs against VL has had an important boost in the last years thanks to the effort done by supra-national entities such as DNDi along with academic institutions and public and private research centers, which have developed campaigns for its rapid eradication from a multidisciplinary perspective. This include from massive screening of new or repurposed molecules in systems with greater translatability, to pre-clinical *in vivo* models that have incorporated new candidates to the initial clinical phases in a short period of time[4,5,6].

The incorporation of modified transgenic parasites that emit light or fluorescence in the presence of specific substrates along with the development of bioimaging detection equipment, have been a great step forward in the progress of preclinical models of VL in experimental animals [7,8,9,10]. The development of *Leishmania* strains stably transfected with the gene encoding firefly luciferase that, in the presence of luciferin, emit light from internal organs, allows real-time analysis of the course of an infection

and its treatment without the need to sacrifice animals [11,12]. Moreover, due to *in vivo* imaging is a friendly, nonlethal procedure, which could be performed repetitively, each animal could be used as its own control, thus reducing the bias caused by animal variability [13]. The good correlation between the parasitic load and the light emitted by the infected organs, and its high sensitivity and reproducibility, have helped to identify dozens of new compounds that are already, or will be in clinical phases shortly[14].

Rodent VL models have served as a previous step to study the disease in other animals such as dogs or non-human primates, and before bridging the gap to early clinical phases in humans [15]. The Balb/c mouse with its innate immunological tolerance to VL has been very useful to mimic the initial phases of the disease and to identify many antileishmanial compounds in a relatively short period of time [12,16]. Although mice infected with *L. donovani* do not die, the use of Balb/c mice has demonstrated to be an adequate model in the study of VL [17,18,19]. As a model that closer resembles the human disease, the hamster is being used because *Leishmania* infection tends to become chronic and can end up killing the animals if they are not treated [20,21]. However, the hamster is too big for the acquisition of internal images after being infected with transgenic parasites, since the conventional light detection systems are not sensitive enough. For this reason, unlike mice, the success of infection in hamsters cannot be verified by bioluminescence until 15 days after infection [19]. To study early stages of the infection it is necessary to rely on more archaic and less ethical methods consisting of the sacrifice of animals at distinct time points and count the parasites that infect internal organs using Giemsa-stained tissue slides. These methods are tedious [16] and, apart from the organs that are expected to be colonized by the parasite (spleen, liver and bone marrow), other tissue compartments or niches, where the parasite would be confined after effective treatment, could be overlooked and could be in the origin of subsequent relapses [8,22].

However, due to its sensitivity and specificity, bioimaging can reveal deep sites of parasite colonization not previously described, which may be useful to explain the host/parasite interplay [22]. The thymus is a primary lymphoid organ that plays a key role in T-cell homeostasis maintenance, which is essential for host CD4+ and CD8+ maturation, that has passed unnoticed as reservoir of *Leishmania* infections[23]. In the

present work, we describe for the first time a chronic model of *L. donovani* VL in Balb/c mice by means of bioimaging techniques aided by qPCR, in which we demonstrate the colonization of lymphoid organs and its validity as an easy-translatable preclinical screening system for new antileishmanial drugs.

Results

We have previously demonstrated the utility of thermostable red-shifted firefly luciferase PpyRE9h as a sensitive reporter for *in vivo* imaging in a chronic mouse model of *L. infantum* VL [12]. The same pLEXSY-PAC-PpyRE9h construct was used to stably integrate the *PpyRE9h* gene into the 18S ribosomal RNA (rRNA) locus of *L. donovani* (MHOM/ET/67/HU3). Puromycin resistant parasites with high luciferase *in vitro* activity were selected for *in vivo* experiments. Once confirmed that the selected clones grew at the same rate as wild-type parasites (data not shown), their infectivity was assessed in Balb/c mice. Mice were i.p. injected with different doses of infective metacyclic promastigotes ($1.5 \times 10^6 – 1.5 \times 10^9$) and photographed at different times post-infection (Fig 1). Only those animals that were infected with a large number of metacyclic parasites ($10^8 – 10^9$), were able to develop a continuous infection detectable by *in vivo* imaging (Fig 1A).

The heat map acquired at 96 h after infection, corresponding to the time needed to transform promastigotes into amastigotes, showed that bioluminescence is spread up all over the body of the animals infected with 10^9 metacyclic promastigotes, while those mice infected with 10^8 metacyclic promastigotes yielded a bioluminescent signal localized in the liver. The other infecting doses (10^6 and 10^7) were undetected under our light acquisition conditions.

Over the next week (1 wpi), most of the bioluminescence signal was seen in the abdominal area near the inoculation site (10^9 infected dose). In addition, light emission was also detected at liver location, along the sternum and two other spots on either side of it. This distribution is more evident at 2-wpi. Over the next three weeks (3-5wpi), the luminescent signal increased mainly in the spleen, which was apparently enlarged and displaced from its original position towards the abdomen, while bioluminescence signals from the liver and sternum remained observable. During last weeks (7-11wpi), the luminescent signal was detected mainly in the spleen location, but not in the location of

the liver. Note that bioluminescence signal was also observed in the sternum of all animals (included those infected with 10^8 parasites), throughout all the experimental period.

The whole-body bioluminescence emitted by mice infected with 10^6–10^7 parasites was close to the background fluorescence emitted by uninfected animals (NI in Fig 1), whereas the total flux recorded from animals infected with a dose of 10^8 parasites was constant over time. Finally, the light emitted by mice infected with 10^9 parasites, peaked at initial time points, decreasing later by 3 wpi to reach values similar to those of the infective dose of 10^8 by weeks 5-11 (Fig. 1B).

In order to obtain more consistent data about the course of infection, we imaged Balb/c mouse (n=15) previously infected intraperitoneally with 10^9 metacyclic parasites (Fig 2A). In addition, with the aim to confirm more accurately the *in vivo* organ distribution of the parasites, especially at the early stage of the infection, cream-depilation of the ventral region of some animals was carried on before imaging acquisition, and different images were taken after applying patches of black modelling clay (Fig. S1) to avoid the interference of the more intense light source over the less potent areas (Fig 2B).

The images acquired during the first week post-infection showed that although the bioluminescent signal spread throughout the body, a more detailed analysis revealed that the hottest spots were located around the lower abdomen, which overlapped with the site of inoculation ("*" in Fig 2A). However, when this location was covered with black modelling clay, other anatomical locations were detected such as liver (red spot in central image at 1 wpi in Fig 2B) and bone marrow (see light signals at the head of femurs and the thoracic light signal emitted by the sternum at 1 wpi in Fig 2B). Furthermore, when the liver signal was also covered (right image at 1 wpi of Fig 2B), two extra spots at both sides of sternum, probably corresponding to the axillary lymph nodes, were clearly detected. The early detection (1wpi) of parasites at long bones, suggests that although the inoculation site was located at the abdomen after intraperitoneal injection, parasites moved rapidly throughout the body.

During 3-4wpi, the bioluminescent signal was still detected all over the body, although clear signals were localized in anatomical regions that include classical target organs

such as liver, spleen, lymph nodes and bone marrow as well as a new location at the thoracic cage, namely the sternum ("**+**" in Figs 2A and 2B).

From 5 wpi onwards, most of the bioluminescent signal was found on the spleen, which enlarged and displaced to the ventral part of abdominal cavity (Fig 2A). The liver signal was hardly detected in whole body images from this moment on (6-11 wpi), but in the group of shaved mice a faint signal could still be detected (see left and central images at 11 wpi in Fig 2B). Moreover, the luminescent signal that had previously been registered in the sternum vanished, being replaced by a clear light spot above the chest at 11wpi, which because of its anatomical position, could correspond to the thymus ("**x**" in Figs 2A and Fig 2B).

Total flux recorded in mice infected with the infective dose of 10^9 increased during the first two weeks and then decreased until 4 wpi, probably reflecting the transition from the acute to the chronic phase of the disease. Finally, from the fourth week onwards the signal remained constant over the tested period (11 weeks). This result agreed well with the results obtained in the previous experiment with the highest infective dose.

Next, we sought the tissue tropism of *PpyRE9h-L. donovani* parasites by *ex vivo* bioluminescent imaging performed on the organs and tissue samples showed in Fig 3A. *Ex vivo* imaging served to identify spleen and liver as the primary sites of *L. donovani* infection using different infective doses (10^9-10^7). However, other locations as mesentery ("*****"in Fig 3B), fat depots around organs ("**→**" in Fig 3B), and thymus ("**×**" in Fig 3B) were also positive, regardless of the dose used.

The finding of unexpected luminescence sources in the mesentery and thorax, moved us to evaluate if the presence of *L. donovani* parasites in such places was a consequence of the inoculation route (i.p. or i.v.) or, on the contrary, were two definitive colonized host tissues. For this purpose, Balb/c mice were infected with 10^9 *L. donovani* metacyclic promastigotes both, intraperitoneally and intravenously and bioluminescence was registered during six weeks. Figure 3C shows that the anatomical distribution of bioluminescence during chronic infection was different. For either of the two infection routes, a clear light signal was observed near the mouse neck, corresponding to the thymus, although it was detected since the first time points in i.p. injected animals while in i.v. injected animals it was delayed to 4 wpi. ("**×**" in Fig 3C). However, the signal

located in the lower abdomen, corresponding to the mesentery, was only detected when mice were i.p. infected ("*" in Fig 3C). *Ex-vivo* imaging confirmed that thymus was positive for bioluminiscence independently of the via used for parasite injection, while bioluminescent signal was only detected in the mesentery of animals infected using the i.p. route (Fig 3D).

In order to confirm microscopically the presence of parasites in the thymus and mesentery, sections of both tissues were stained with Giemsa dye (Fig 4A). Amastigotes were observed intracellularly in several cells of both tissues ("→"in Figure 4A). In the thymus, intracellular amastigotes were located in the medullar area. In addition, to study the course of the infection in thymus, we sacrificed Balb/c mice at different times and their thymus were dissected for *ex vivo* imaging and parasite quantification. Figure 4 shows that *L. donovani* parasites started thymus colonization from the beginning (1wpi) of the infection. Surprisingly, at 3 wpi the parasite burden slightly decreased (not significative) and then spread up again until the infection was stabilized (8wpi) (Figs 4B and 4C).

Next, we assessed the capability of this chronic model of *L. donovani* VL to evaluate the *in vivo* efficacy of new drugs using miltefosine as proof of concept. Because of the bioluminescence signal decreases during the acute phase of infection, the animals were treated once the chronic phase of infection was clearly established and most of the bioluminescent signal was located at the anatomical region of the spleen (starting at 6 wpi). We used two doses of miltefosine (40 mg/kg/day and 10 mg/kg/day) for 5 consecutive days administered by oral gavage. Images of the animals were taken before the starting of the treatment (image 1 on the first day of treatment), on day 8 (image 2) and on day 12 (image 3) (Fig 5A).The second and third images were acquired 72 h after the end of treatment (day 8 from the beginning of treatment) and 7 day after the end of treatment (day 12 from the beginning of treatment) to evaluate the effect of miltefosine (Fig 5A).

Miltefosine (40 mg/kg/d for 5 days) led to a significative and sharp reduction of bioluminescence close to background levels at both time points examined (reductions of 98.33% and 98.51% at 72 h and 7 days after the end of the treatment, respectively) (Figs 5B and 5C), while the lower dose of miltefosine (10 mg/kg/d for 5 days) also

produced a significant reduction in luminescence on day 8 that was more evident on day 12 (reductions of 90.56% and 94.58%, respectively) (Fig 5B). Total flux showed that the bioluminescent signal obtained from the image 2 (72h after the end of treatment) and 3 (7 days after the end of treatment) was stable, suggesting that the infection did not recover up (Fig 5C).

After imaging, the animals on day 12 were sacrificed and different organs and tissues were collected for *ex vivo* imaging and parasite load quantification. The highest *ex vivo* bioluminescent signal was detected in the spleen, followed by the liver, thymus, mesentery and fat depots around the kidney, confirming previous results (Fig 5D). Although both doses of miltefosine (40 and 10 mg/kg/d) were able to prevent the *in vivo* emission of bioluminescence (Fig 5B), the *ex vivo* isolated organs still emitted light (Fig 5D). It is worth noting that the reduction of the spleen weight produced by the treatments, suggesting a direct activity of miltefosine on spleen inflammation.

The parasitic burden in organs and tissues was quantified by qPCR using the primers and temperature ramps described in Material and Methods to specifically amplify *L. donovani* kinetoplastid DNA (kDNA). The results shown in Fig 5E confirmed the reduction of the parasitic load at both doses of miltefosine in all analysed organs (estimated between 97.91% and 99.99%), although the reduction at 40 mg/kg/d was slightly higher than that found at 10 mg/kg/d (Fig 5E).

Since miltefosine was not able to clear completely parasites from organs, we assayed whether cyclophosphamide (CPP) induced immunosuppression could enhance the reactivation of any residual parasite. The experiment was performed as described before: chronic infected animals (image1) were treated with miltefosine 40 mg/kg/d for 5 consecutive days and once the bioluminescent signal disappeared (image 2), animals were immunosuppressed, one month after finishing the treatment with miltefosine (corresponding to one miltefosine half-life) (Fig 6A). The last images (image 3) were taken 72 h after the end of immunosuppression treatment and before euthanasia. Miltefosine was highly effective on chronic VL infections with 7/10 mice remaining bioluminescent negative after immunosuppression (Figs 6B and 6C).

Ex vivo imaging showed reduction in bioluminescence in all organs after miltefosine treatment that was slightly reverted in spleen after CPP immunosuppression (Fig 6D).

qPCR measurement of tissue-specific parasite burdens confirmed miltefosine efficacy in all organs with parasite burden reductions ranging between 95.87% and 99.81% that remained unchanged after immunosuppression (Fig 6E).

Finally, we looked for a correlation between the parasitic load in the different organs and tissues of the infected mice through qPCR and the specific bioluminescence of such tissues both, *ex vivo* and *in vivo*. Figure 7 shows a clear correlation between qPCR-parasite burden and *ex vivo* bioluminescent signal in spleen, liver and thymus. On the contrary, the *in vivo* bioluminescent data were more difficult to correlate with the exception of the spleen. In our model of VL, the infection caused the swelling and displacement of the spleen to the ventral area of mouse abdomen. These changes facilitated *in vivo* identification of the bioluminescent region of interest in this organ, unlike the liver and thymus, whose deeper anatomical location made it more difficult.

Discussion

Infection of Balb/c mice with *L. donovani* parasites serves as a model for the clinical spectrum of human VL [17]. The infection in the liver is acute and self-resolves by developing a CD4+T cell-dependent immune response with the formation of granulomas, these features being found in asymptomatic human patients [24]. On the contrary, the spleen remains chronically infected with tissue pathology and immune dysfunction, which is similar to what is found in VL patients [25].

For experimental VL in susceptible mice, different inoculation routes and parasite dose could be responsible for the development of protective versus suppressive adaptive immune responses [18].

Experimental murine model of VL frequently uses intravenous or intraperitoneal injection of high-dose (10^7 and higher) of *L. donovani* or *L. infantum* amastigotes, although more natural infections using low-dose intradermal infections have also been described [26]. We have infected Balb/c mice intraperitoneally with a high-dose (10^8-10^9) of *PpyRE9h-L. donovani* metacyclic promastigotes to study the course of infection in individual Balb/c mice throughout several months for *in vivo* systematic drug efficacy testing under chronic infection conditions when murine spleen is highly compromised. Tissue-specific parasite loads were then quantified and correlated with *ex vivo* and *in*

vivo bioluminescent imaging data so as to infer parasite loads and accelerate the initial stages of drug discovery in murine models of VL.

The *in vivo* imaging approach allows longitudinal monitoring in individual mice along with reduction of the number of animals required, since parasite burden can be inferred from the *in vivo* evaluation [19,27,28,29]. Thereby, it is not necessary to systematically slaughter animals to assess parasite load, unless we find very highly effective drugs that extremely reduces parasite load below the *in vivo* bioluminescent threshold. In this way, we can focus mainly on potentially promising molecules and increase the tested drug rate.

In order to infect mice, we have used metacyclic parasites grown over 7 days in rich medium supplemented with 20% FBS, and the cultures were permanently maintained with gentle agitation, thus large numbers of parasites/mL were reached ($130x10^6$). On day 7, most of parasites are still motile, but other non-motile parasites, probably apoptotic parasites, can also be seen. Although intravenous and intraperitoneal administration routes are the most frequently used, the latter was chosen because it is associated to more homogeneous infections [30]. This allowed us to infect a high number of animals (>30) in order to make groups of 5 mice that comprised not only the positive control – usually miltefosine administered by oral gavage – but also the vehicles and drugs to be tested. Thereby, we can test at least 3 drugs or concentrations, simultaneously.

To validate the model, miltefosine (the unique oral drug used against VL), was used. The treatment was initiated once chronic infection was established (6 weeks post-infection) using two doses (40 and 10 mg/kg) daily for five days. *In vivo* bioluminescent signal dropped at 72 h after the end of treatment, although a weak signal still remained. This trend was maintained one week after the end of treatment, when the bioluminescent signal was below the camera's threshold, probably due to the long miltefosine half-life (>30 days) [31].

Although at that time *in vivo* imaging showed a lack of signal, *ex vivo* organ imaging revealed the persistence of parasites in all organs. The parasitic load estimated by qPCR in the liver, spleen, thymus and bone marrow correlated well with the *in vivo* and *ex vivo* bioluminescence values. Therefore, the light intensity emitted by these organs is a good

parameter to follow the course of the parasitic infection and drug efficacy against the infection.

The data confirmed that there was no-sterile cure as previously described in mice [32,33,34,35]. Therefore, the next question that came up was whether those parasites still remaining in the organs could generate a new infection in an immunocompromised scenario. However, immunosuppression after treatment with CPP did not show any significant change in the parasitic load of these animals.

Surprisingly, our model allowed us to describe two previously non-reported organs for leishmania parasites; the thymus and the mesentery, which could be the source of subsequent relapses. The latter, was not detected after intravenous administration, and therefore, it could probably be an artefact due to the intraperitoneal administration of the parasites. However, this unexpected location can provide an early storage of parasites that gradually disappear over time, probably due to the activation of peritoneal macrophages. Recently, the presence of parasites in the peritoneal cavity has been described after intraperitoneal administration of promastigotes [36]. The bioluminescent signal detected in the peritoneal cavity after intraperitoneal infection was difficult to quantify due to the photons emitted by organs such as the spleen or liver masked other organs infected nearby. However, the use of black plaster patches to avoid the bright emission from some areas enabled us to clearly observe the location of the parasites in less brilliant organs.

On the contrary, the thymus appeared consistently infected as a result of both intraperitoneal and intravenous administration routes. To our knowledge, there is no report describing thymus infection in VL patients. However, this organ is targeted by many different pathogens responsible for chronic infections, such as viruses, bacteria, fungi and also by closely related protozoans as *Trypanosoma cruzi* [37]. In the context of *Leishmania* infections, the presence of *L. infantum* parasites in the thymus has been recently described in an experimental setting with Balb/c mice fed with low protein diet [38] as well as in naturally infected dogs from endemic areas in Brazil [23].

Colonization of the thymus by *L. donovani* was observed from the beginning of the infection (1 wpi), and then remained chronically from that moment on, as described in infections caused by *Mycobacterium*[39]. The slight decrease of the parasitic load (not

significant) observed in the third week after the infection, which probably corresponds to a failed attempt to control the infection, differs from what occurs in systemic *Salmonella* infections, in which the thymus was able to clear the bacteria[40].

Thymus is the central organ that receives hematopoietic cells from bone marrow and induces central tolerance by positive and negative clonal deletion of autoreactive thymocytes, thus surviving those thymocytes that recognize self-peptide-MHC [41]. Thymus is also the organ where regulatory T-cells (Treg) develop, the latter playing key roles in the prevention of autoimmunity and the maintenance of immune homeostasis [42]. One of the most common immunological consequences of pathogen infections is the impairment of the central tolerance process in thymocytes, thus affecting both positive and negative selection processes [43]. We have identified parasites at the medullar level of the thymus, which is reasonable because the cortex is protected from the influence of circulating antigens by a blood-thymus barrier[44]. In addition, the perimedullary cortex is known to be the region of the thymus where bone marrow cells continually enter the organ[45]. It is then reasonable to hypothesize that the parasites could reach the medullary region of the thymus either directly from the bloodstream or engulfed within macrophages and dendritic cells from the infected bone marrow.

On the other hand, knowing which cells in the thymic environment are affected, might help predict the effects the infection is responsible for; either emigration of immature T cells, if conventional T cells are affected, or impaired pathogen clearance if T-reg are affected.

Experimental section

Animals

Six to eight weeks old female Balb/c mice were purchased from Janvier Labs (St Berthevin Cedex, France). All the *in vivo* experiments described in this manuscript were conducted in compliance with Spanish Act (RD 53/2013) and European Union Legislation (2010/63/UE). The protocols were approved by the Animal Care Committee of the Universidad de León (ULE, León, Spain), project license number 2019/07.

Animals were housed individually in ventilated cages, under specific pathogen-free conditions in the P2-facility of ULE. Mice were maintained on a 12 h light/dark cycle and had access to food and water *ad libitum*.

Parasites

L. donovani (strain MHOM/ET/67/HU3) promastigotes were routinely cultured at 26 °C in Schneider´s insect medium (Sigma-Aldrich) supplemented with 20% (v/v) heat-inactivated fetal bovine serum (FBS) and antibiotic cocktail (200 U/mL penicillin, 200 µg/mL streptomycin).

Animal infection

Parasites for infecting animals were obtained from splenic amastigotes as previously described [9]. Stationary phase *PpyRE9h + L. donovani* promastigotes were collected by centrifugation (4,400 rpm, 15 min) and washed three times with PBS. Mice were infected with different parasite doses (ranging from 1.5×10^6 to 1.5×10^9 promastigotes) by intraperitoneal route or with a standarized dose of 1.5×10^8 by intravenous route.

Bio-luminescent imaging

At different time points of the infection, D-luciferin (PerkinElmer, Walthan, MA, USA) was injected subcutaneously to Balb/c mice at a dose of 150 mg/kg body weight. Animals were anaesthetized with 2.5% (vol/vol) gaseous isofluorane in oxygen, subsequently reduced to 1.5 %. To measure bioluminescence, mice were placed in an IVIS Spectrum device (PerkinElmer) and a sequence of bioluminescence images was acquired (each photograph was captured every 2 min during a total time of 30 min) according to the following acquisition parameters: exposure time Auto, binning 8 and f/stop 1. After imaging, mice were removed from the anesthesia and returned to their cages where awoke spontaneously. Bioluminiscence was quantified for all images of the acquired sequence and was expressed as total flux (photons/s; p/s). To estimate parasite burden, whole body regions of interest (RoI) were drawn using Living Image software (PerkinElmer) to quantify bioluminescence expressed as total flux (photons/s). To standardize the results, the quantifications showed in the figures correspond to the maximum signal emitted by each mouse. Uninfected mice were used to estimate the detection threshold for *in vivo* imaging. Finally, at the end of the experiments, animals

were euthanized and dissected to obtain their organs, which were imaged in the IVIS Spectrum system after having been immersed in a solution of 15 mg/mL D-luciferin in PBS. To establish a correlation between the maximum bioluminescence signal emitting by organs both *ex vivo* and *in vivo*, RoI were drawn around the corresponding organs and bioluminescence was expressed as total flux (photons/s) too.

Histology

Tissue samples were fixed in 10% buffered formalin for 48-72h, dehydrated, cleared and embedded in paraffin. Sections (2 µm) were incubated with Giemsa stain (Sigma-Aldrich) (1:3, vol/vol in water) for 30 min. All images were taken with a E600 (Nikon) light microscope.

Drug treatment

Eight weeks after infection, mice were randomly divided into groups of five. Miltefosine (Sigma-Aldrich) was dissolved in water and was administered in regimens of 40 and 10 mg/kg of body weight daily for 5 days by oral gavage (200 µL). To detect residual infection, mice were immunosuppressed with cyclophosphamide monohydrate (Sigma-Aldrich) (200 mg/kg) injected intraperitoneally every 3 days for a maximum of 3 doses.

Quantification of parasite burden by qPCR

After completing the different treatments, animals were euthanized and dissected in sterile conditions. Liver, spleen, thymus and bone marrow were snap frozen on dry ice and stored at −20°C. DNA was extracted using EXTRACTME DNA tissue kit (EM03) (Blirt SA, Poland) following manufacturer's instructions. To quantify the number of parasites, a set of specific primers targeted at 116-bp template of the kinetoplastid DNA of *L. donovani* was used [46]. qPCR reactions were prepared using the PowerUp™ SYBR™ Green Master Mix (Applied Biosystems™) and run on a StepOnePlus™ qPCR instrument, (Applied Biosystems™). Each reaction contained 1 µL of extracted DNA in 19 µL reaction mix containing 1x SYBR Green Master mix and 50 nM of each primer (forward 5´-GGGTAGGGGCGTTCTGCGAAA-3´; reverse 5´-CCTATTTTACACCAACCCCCAGT-3´) in nuclease-free water. Measurements of *L. donovani* DNA content were normalized using the ratio of Ct values for *L. donovani* - and mouse-specific non-infected tissues and converted to estimated numbers of parasite equivalents by reference to a standard

curve with a range of 1×10^7– 1×10^2 parasite equivalents/mL. Thermal cycling profile was as follows: 50°C for 2 min, 95°C for 2 min, 40 cycles at 95°C for 15 s and 64°C for 30 s, followed by a melt curve, from 64°C to 95°C. Finally, the number of parasites per milligram of tissue was calculated using StepOne™ Software. The limit of detection of this protocol is 10 parasites per milligram of tissue.

Statistics

One-way analysis of variance (ANOVA) and Tukey's multiple-comparison were used to evaluate the differences between groups. Differences with a P value < 0.05 were considered statistically significant. For statistical analyses, GraphPad Prism version 5.0 software (GraphPad Software, Inc., San Diego, CA) was used.

Corresponding Author Information: rmregt@unileon.es; rbalf@unileon.es

ORCIDs:

Bárbara Domínguez Asenjo: 0000-0002-3474-3422

Camino Gutiérrez Corbo: 0000-0002-3626-3457

Rosa M Reguera: 0000-0001-9148-2997

Rafael Balaña-Fouce 0000-0003-0418-6116

Yolanda Pérez-Pertejo: 0000-0003-2361-3785

Salvador Iborra: 0000-0002-1607-1749

Author Contributions: BDA performed the experiments, acquisition, analysis, interpretation of data and wrote the paper. RMR and RBF edited the manuscript and provided scientific input. CGG, YPP, RBF and RRT helped in conceptualizing the idea, interpretation of data, and editing of the draft.

ACKNOWLEDGMENTS. The first author BDA as well as CGC are recipients of Junta de Castilla y Leon (JCyL) and European Social Found (ESF)'s Fellowships Scheme for Doctoral Training Programs. The IVIS® Spectrum Imaging System was purchased as part of

INFRARED program (2018-ULE1) of Junta de Castilla y Leon (JCyL) funded by European Regional Development Fund (ERDF). The authors would like to thank Miguel Fernández Fernández and other members of the Animal House of University of León for their impeccable care of the animals. This collaborative research was funded by MINECO; SAF2017-83575-R to RMR.

REFERENCES

(1) Esch, K. J., and Petersen, C. A. (2013) Transmission and epidemiology of zoonotic protozoal diseases of companion animals. *Clin. Microbiol. Rev.* 26, 58–85. DOI: 10.1128/CMR.00067-12.

(2) Burza, S., Croft, S. L., and Boelaert, M. (2018) Leishmaniasis. *Lancet* 392, 951–970. DOI: 10.1016/S0140-6736(18)31204-2.

(3) Roatt, B. M., de Oliveira Cardoso, J. M., De Brito, R. C. F., Coura-Vital, W., de Oliveira Aguiar-Soares, R. D., and Reis, A. B. (2020) Recent advances and new strategies on leishmaniasis treatment. *Appl. Microbiol. Biotechnol.* 104, 8965–8977. DOI: 10.1007/s00253-020-10846-y.

(4) Don, R., and Ioset, J. R. (2014) Screening strategies to identify new chemical diversity for drug development to treat kinetoplastid infections. *Parasitology* 141, 140–146. DOI: 10.1017/S003118201300142X

(5) Balaña-Fouce, R., Pérez Pertejo, M. Y., Domínguez-Asenjo, B., Gutiérrez-Corbo, C., and Reguera, R. M. (2019) Walking a tightrope: drug discovery in visceral leishmaniasis. *Drug Discov. Today* 24, 1209–1216. DOI: 10.1016/j.drudis.2019.03.007.

(6) Bhattacharya, A., Corbeil, A., Do Monte-Neto, R. L., and Fernandez-Prada, C. (2020) Of drugs and Trypanosomatids: new tools and knowledge to reduce bottlenecks in drug discovery. *Genes* 11, 1–24. DOI: 10.3390/genes11070722.

(7) Millington, O. R., Myburgh, E., Mottram, J. C., and Alexander, J. (2010) Imaging of the host/parasite interplay in cutaneous leishmaniasis. *Exp. Parasitol.* 126, 310–317. DOI: 10.1016/j.exppara.2010.05.014.

(8) Calvo-Álvarez, E., Guerrero, N. A., Álvarez-Velilla, R., Prada, C. F., Requena, J. M., Punzón, C., Llamas, M. Á., Arévalo, F. J., Rivas, L., Fresno, M., Pérez-Pertejo, Y., Balaña-Fouce, R., and Reguera, R. M. (2012) Appraisal of a *Leishmania major* strain stably expressing mCherry fluorescent protein for both *in vitro* and *in vivo* studies of potential drugs and vaccine against cutaneous leishmaniasis. *PLoS Negl. Trop. Dis.* 6, e1927. DOI: 10.1371/journal.pntd.0001927.

(9) Calvo-Álvarez, E., Stamatakis, K., Punzón, C., Álvarez-Velilla, R., Tejería, A., Escudero-Martínez, J. M., Pérez-Pertejo, Y., Fresno, M., Balaña-Fouce, R., and Reguera,

R. M. (2015) Infrared fluorescent imaging as a potent tool for *in vitro*, *ex vivo* and *in vivo* models of visceral leishmaniasis. *PLoS Negl. Trop. Dis.* 9, e0003666. DOI: 10.1371/journal.pntd.0003666.

(10) Avci, P., Karimi, M., Sadasivam, M., Antunes-Melo, W. C., Carrasco, E., and Hamblin, M. R. (2018) *In-vivo* monitoring of infectious diseases in living animals using bioluminescence imaging. *Virulence* 9, 28–63. DOI: 10.1080/21505594.2017.1371897.

(11) Lang, T., Goyard, S., Lebastard, M., and Milon, G. (2005) Bioluminescent *Leishmania* expressing luciferase for rapid and high throughput screening of drugs acting on amastigote-harbouring macrophages and for quantitative real-time monitoring of parasitism features in living mice. *Cell Microbiol.* 7, 383–392. DOI: 10.1111/j.1462-5822.2004.00468.x.

(12) Álvarez-Velilla, R., Gutiérrez-Corbo, M. C., Punzón, C., Pérez-Pertejo, M. Y., Balaña-Fouce, R., Fresno, M., and Reguera, R. M. (2019) A chronic bioluminescent model of experimental visceral leishmaniasis for accelerating drug discovery. *PLoS Negl. Trop. Dis.* 13, e0007133. DOI: 10.1371/journal.pntd.0007133.

(13) Lang, T., Lecoeur, H., and Prina, E. (2009) Imaging *Leishmania* development in their host cells. *Trends Parasitol.* 25, 464–473. DOI: 10.1016/j.pt.2009.07.006.

(14) Van Bocxlaer, K., Caridha, D., Black, C., Vesely, B., Leed, S., Sciotti, R. J., Wijnant, G. J., Yardley, V., Braillard, S., Mowbray, C. E., Ioset, J. R., and Croft, S. L. (2019) Novel benzoxaborole, nitroimidazole and aminopyrazoles with activity against experimental cutaneous leishmaniasis. *Int. J. Parasitol. Drugs Drug Resist.* 11, 129–138. DOI: 10.1016/j.ijpddr.2019.02.002.

(15) Novobilský, A., and Höglund, J. (2020) Small animal *in vivo* imaging of parasitic infections: a systematic review. *Exp. Parasitol.* 214, 107905. DOI: 10.1016/j.exppara.2020.107905.

(16) Gupta, S., and Nishi. (2011) Visceral leishmaniasis: experimental models for drug discovery. *Indian J. Med. Res.* 133, 27–39.

(17) Kaye, P. M., Svensson, M., Ato, M., Maroof, A., Polley, R., Stager, S., Zubairi, S., and Engwerda, C. R. (2004) The immunopathology of experimental visceral leishmaniasis. *Immunol. Rev.* 201, 239–253. DOI: 10.1111/j.0105-2896.2004.00188.x.

(18) Loeuillet, C., Bañuls, A. L., and Hide, M. (2016) Study of *Leishmania* pathogenesis in mice: experimental considerations. *Parasit. Vectors* 9, 144. DOI: 10.1186/s13071-016-1413-9.

(19) Melo, G. D., Goyard, S., Lecoeur, H., Rouault, E., Pescher, P., Fiette, L., Boissonnas, A., Minoprio, P., and Lang, T. (2017) New insights into experimental visceral leishmaniasis: real-time in vivo imaging of *Leishmania donovani* virulence. *PLoS Negl. Trop. Dis.* 11, e0005924. DOI: 10.1371/journal.pntd.0005924.

(20) Rouault, E., Lecoeur, H., Meriem, A. B., Minoprio, P., Goyard, S., and Lang, T. (2017) Imaging visceral leishmaniasis in real time with golden hamster model: monitoring the parasite burden and hamster transcripts to further characterize the immunological responses of the host. *Parasitol. Int.* 66, 933–939. DOI: 10.1016/j.parint.2016.10.020.

(21) Saini, S., and Rai, A. K. (2020) Hamster, a close model for visceral leishmaniasis: opportunities and challenges. *Parasite Immunol.* 42, e12768. DOI: 10.1111/pim.12768.

(22) Capewell, P., Cren-Travaillé, C., Marchesi, F., Johnston, P., Clucas, C., Benson, R. A., Gorman, T. A., Calvo-Alvarez, E., Crouzols, A., Jouvion, G., Jamonneau, V., Weir, W., Lynn Stevenson, M., O'Neill, K., Cooper, A., Swar, N. R. K., Bucheton, B., Ngoyi, D. M., Garside, P., Rotureau, B., and MacLeod, A. (2016) The skin is a significant but overlooked anatomical reservoir for vector-borne African trypanosomes. *Elife* 5, e17716. DOI: 10.7554/eLife.17716.

(23) da Silva, A. V. A., de Souza, T. L., Figueiredo, F. B., Mendes, A. A. V., Ferreira, L. C., Filgueira, C. P. B., Cuervo, P., Porrozzi, R., Menezes, R. C., and Morgado, F. N. (2020) Detection of amastigotes and histopathological alterations in the thymus of *Leishmania infantum*-infected dogs. *Immun. Inflamm.* 8, 127–139. DOI: 10.1002/iid3.285.

(24) Stanley, A. C., and Engwerda, C. R. (2007) Balancing immunity and pathology in visceral leishmaniasis. *Immunol. Cell Biol.* 85, 138–147. DOI: 10.1038/sj.icb7100011.

(25) Engwerda, C. R., and Kaye, P. M. Organ-specific Immune responses associated with infectious disease. *Immunol. Today* 21, 73–78. DOI: 10.1016/s0167-5699(99)01549-2.

(26) Ahmed, S., Colmenares, M., Soong, L., Goldsmith-Pestana, K., Munstermann, L., Molina, R., and McMahon-Pratt, D. (2003) Intradermal infection model for pathogenesis and vaccine studies of murine visceral leishmaniasis. *Infect. Immun.* 71, 401–410. DOI: 10.1128/iai.71.1.401-410.2003.

(27) Thalhofer, C. J., Graff, J. W., Love-Homan, L., Hickerson, S. M., Craft, N., Beverley, S. M., and Wilson, M. E. (2010) *In vivo* imaging of transgenic leishmania parasites in a live host. *J. Vis. Exp.* 41, 1980. DOI: 10.3791/1980.

(28) Michel, G., Ferrua, B., Lang, T., Maddugoda, M. P., Munro, P., Pomares, C., Lemichez, E., and Marty, P. (2011) Luciferase-expressing *Leishmania infantum* allows the monitoring of amastigote population size, *in vivo*, *ex vivo* and *in vitro*. *PLoS Negl. Trop. Dis.* 5, e1323. DOI: 10.1371/journal.pntd.0001323.

(29) Tavares, J., Costa, D. M., Teixeira, A. R., Cordeiro-da-Silva, A., and Amino, R. (2017) *In vivo* imaging of pathogen homing to the host tissues. *Methods* 127, 37–44. DOI: 10.1016/j.ymeth.2017.05.008.

(30) Rolão, N., Melo, C., and Campino, L. (2004) Influence of the inoculation route in Balb/c mice infected by *Leishmania Infantum*. *Acta Trop.* 90, 123–126. DOI: 10.1016/j.actatropica.2003.09.010.

(31) Breiser, A., Kim, D. J., Fleer, E. A. M., Damenz, W., Drube, A., Berger, M., Nagel, G. A., Eibl, H., and Unger, C. (1987) Distribution and metabolism of hexadecylphosphocholine in mice. *Lipids* 22, 925–926. DOI: 10.1007/BF02535556.

(32) Kuhlencord, A., Maniera, T., Eibl, H., and Unger, C. (1992) Hexadecylphosphocholine: oral treatment of visceral leishmaniasis in mice. *Antimicrob. Agents Chemother*. 36, 1630–1634. DOI: 10.1128/aac.36.8.1630.

(33) Escobar, P., Yardley, V., and Croft, S. L. (2001) Activities of hexadecylphosphocholine (miltefosine), Ambisome, and sodium stibogluconate (Pentostam) against *Leishmania donovani* in immunodeficient scid mice. *Antimicrob. Agents Chemother.* 45, 1872–1875. DOI: 10.1128/AAC.45.6.1872-1875.2001.

(34) Fortin, A., Hendrickx, S., Yardley, V., Cos, P., Jansen, H., and Maes, L. (2012) Efficacy and tolerability of oleylphosphocholine (OLPC) in a laboratory model of visceral leishmaniasis. *J. Antimicrob. Chemother.* 67, 2707–2712. DOI: 10.1093/jac/dks273.

(35) Mendes Costa, D., Cecílio, P., Santarém, N., Cordeiro-da-Silva, A., and Tavares, J. (2019) Murine Infection with bioluminescent *Leishmania infantum* axenic amastigotes applied to drug discovery. *Sci. Rep.* 9, 18989. DOI: 10.1038/s41598-019-55474-3.

(36) Ong, H. B., Clare, S., Roberts, A. J., Wilson, M. E., and Wright, G. J. (2020) Establishment, optimisation and quantitation of a bioluminescent murine infection model of visceral leishmaniasis for systematic vaccine screening. *Sci. Rep.* 10, 4689. DOI: 10.1038/s41598-020-61662-3.

(37) Savino, W. (2006) The thymus is a common target organ in infectious diseases. *PLoS Pathog*. 2, e62. DOI: 10.1371/journal.ppat.0020062.

(38) Losada-Barragán, M., Umaña-Pérez, A., Durães, J., Cuervo-Escobar, S., Rodríguez-Vega, A., Ribeiro-Gomes, F. L., Berbert, L. R., Morgado, F., Porrozzi, R., Mendes-Da-cruz, D. A., Aquino, P., Carvalho, P. C., Savino, W., Sánchez-Gómez, M., Padrón, G., and Cuervo, P. (2019) Thymic microenvironment is modified by malnutrition and *Leishmania Infantum* Infection. *Front. Cell. Infect. Microbiol.* 9, 252. DOI: 10.3389/fcimb.2019.00252.

(39) Nobrega, C., Cardona, P. J., Roque, S., Pinto do Ó, P., Appelberg, R., and Correia-Neves, M. (2007) The thymus as a target for mycobacterial infections. *Microbes Infect.* 9, 1521–1529. DOI: 10.1016/j.micinf.2007.08.006.

(40) Ross, E. A., Coughlan, R. E., Flores-Langarica, A., Lax, S.; Nicholson, J., Desanti, G. E., Marshall, J. L., Bobat, S., Hitchcock, J., White, A., Jenkinson, W. E.; Khan, M., Henderson, I. R., Lavery, G. G., Buckley, C. D., Anderson, G., and Cunningham, A. F. (2012) Thymic function is maintained during *Salmonella*-induced atrophy and recovery. *J. Immunol.* 189, 4266–4274. DOI: 10.4049/jimmunol.1200070.

(41) Audiger, C., Rahman, M. J., Yun, T. J., Tarbell, K. V., and Lesage, S. (2017) The importance of dendritic cells in maintaining immune tolerance. *J. Immunol.* 198, 2223–2231. DOI: 10.4049/jimmunol.1601629.

(42) Savage, P. A., Klawon, D. E. J., and Miller, C. H. (2020) Regulatory T cell development. *Annu. Rev. Immunol.* 38, 421–453. DOI: 10.1146/annurev-immunol-100219-020937.

(43) Nunes-Alves, C., Nobrega, C., Behar, S. M., and Correia-Neves, M. (2013) Tolerance has its limits: how the thymus copes with infection. *Trends Immunol.* 34, 502–510. DOI: 10.1016/j.it.2013.06.004.

(44) Raviola, E., and Karnovsky, M. J. (1972) Evidence for a blood-thymus barrier using electron-opaque tracers. *J. Exp. Med.* 136, 466–498. DOI: 10.1084/jem.136.3.466.

(45) Lind, E. F., Prockop, S. E., Porritt, H. E., and Petrie, H. T. (2001) Mapping precursor movement through the postnatal thymus reveals specific microenvironments supporting defined stages of early lymphoid development. *J. Exp. Med.* 194, 127–134. DOI: 10.1084/jem.194.2.127.

(46) Srivastava, A., Sweat, J. M., Azizan, A., Vesely, B., and Kyle, D. E. (2013) Real-time PCR to quantify *Leishmania donovani* in hamsters. *J. Parasitol.* 99, 145–150. DOI: 10.1645/GE-3221.1.

CAPTIONS TO FIGURES

Figure 1. Course of the visceral infection after inoculating different doses of *PpyRE9h* luciferase-expressing *L. donovani* metacyclic promastigotes.

A. Representative ventral images of Balb/c mice infected with several doses of metacyclic parasites (10^6-10^9). Heat-maps are scaled on log10, indicating the bioluminescence signal from low (blue) to high (red). The minimum and maximum radiances for the pseudocolour scale are indicated.

B. Quantification of total ventral bioluminescence of whole-body infected mice, expressed as total flux (photons/s), from the experiment represented in panel A.

Figure 2. Progression of PpyRE9h + *L. donovani* infection over the time.

A. Representative ventral view images of Balb/c mice sequentially taken at different time points over 11 weeks after i.p. inoculation of 1.5×10^9 PpyRE9h *L. donovani* metacyclic parasites (representative of n = 4-10 mice per experiment). "*" indicates the place of inoculation; "+" indicates the expected organs targeted by *L. donovani*, such as liver, spleen, lymph nodes and bone marrow. The new location along the chest, which was later replaced by a bright spot on the sternum is identified with "x".

B. In vivo images of the same Balb/c infected mouse that had been shaved in the ventral region in order to locate new anatomical sources of luminescence. "*" indicates the place of inoculation; "+" indicates the expected target organs "x" indicates the new location in the thoracic cage.

C. Quantification of the total bioluminescence of whole-body infected mice, expressed as total flux (photons/s), of the experiment represented in panel A. Means ± SD (n= 4-10 animals) are represented. The gray line indicates the detection threshold determined as the mean (solid line) of the background luminescence of the non-infected control mice. The averages of each time are indicated as red lines.

Figure 3. Tissue tropism analysis of PpyRE9h + *L. donovani* strain in Balb/c mice.

A. Representative display of the organs that were imaged *ex vivo*, at the end of the experiments (top left). Balb/c mice infected with several doses of metacyclic parasites (10^6-10^9). "*" mesentery, "x" thymus and "→" fat depots around kidney (top right).

B. Representative ventral images of Balb/c mice taken at sequential time points over the course of 6 weeks after i.p. or i.v. inoculation of 1.5×10^8 PpyRE9h + *L. donovani*."+" thymus and "*" parasite´s inoculation sites.

C. *Ex vivo* imaging of thymus and intestine of Balb/c mice i.p. or i.v. infected with 1.5×10^8 PpyRE9h + *L. donovani* metacyclic promastigotes.

D. *Ex vivo* imaging of thymus and intestine of Balb/c mice infected intraperitoneally (left) or intravenously (right) with 1.5×10^8 *PpyRE9h + L.donovani* promastigotes.

Figure 4. Progression of the parasite colonization of thymus dissected from mice infected with PpyRE9h + *L. donovani*.

A. Giemsa staining of thymus sections obtained from infected with PpyRE9h + L. donovani after 11 weeks of infection ("→" amastigotes).

B. *Ex vivo* imaging of thymus isolated from Balb/c mice infected intraperitoneally with 1.5×10^9 promastigotes, at different times.

C. Parasite burdens estimated by qPCR from mouse thymus sacrificed at 1, 2, 3 and 8 wpi. Each point represents the mean ± SD of n=3 individuals. Statistical significance was calculated by one-way ANOVA test: (*P < 0.05; **P < 0.01; ***P < 0.001).

Figure 5. Treatment of chronic *L. donovani* infection with 40 mg/kg/d (MTF40) and 10 mg/kg/d miltefosine (MTF10) for 5 consecutive days by oral gavage in Balb/c mice.

A. Schematic representation of the experimental design. Animals were i.p. infected with 10^9 *L. donovani* metacyclic promastigotes and after 6 wpi were orally treated with MTF40 or MTF10 for 5 consecutive days (blue). Mice were then imaged before starting the treatment (image 1), 72 h (image 2) and 7 days after the end of treatment (image 3). At the last time point animals were sacrificed and the parasite burden of the liver, spleen, bone marrow and thymus were determined by qPCR.

B. Representative ventral images of Balb/c mice after treatment with MTF40 and MTF10 for 5 consecutive days at several time points Mice were imaged before starting the treatment (image 1), 72 h after (image 2) and 7 days after the end of treatment (image 3). (Unt) represents the animals treated only with the drug vehicle (water). Images are representative of *n* = 3–5 individuals per experiment.

C. Quantification of whole ventral bioluminescence, expressed as total flux (photons/s), from the experiment. Each point represents means ± SD of n individuals. (Unt) group was imaged for quantification of luminescence background (grey dashed line). Statistical significance calculated by one-way ANOVA: (*P < 0.05; **P < 0.01; ***P < 0.001).

D. Ex vivo images of mice organs after treatment with MTF40 or MTF10 for 5 consecutive days. Untreated mice (Unt), Lung (Lu), Liver (Li), Spleen (S), Heart (H), Kidney (K), Thymus (T) and Intestine (I).

E. Parasite burdens estimated by qPCR in untreated (Unt) and MTF40 or MTF10 for 5 consecutive days on liver, spleen, bone marrow and thymus. Each point represents means ± SD of n animals. Statistical significance calculated by one-way ANOVA: (*P < 0.05; **P < 0.01; ***P < 0.001).

Figure 6. Effect of an immune suppressive treatment with cyclophosphamide (CPP) after MTF40 treatment of chronic *L. donovani* mouse VL.

A. Schematic representation of the experimental design. Balb/c mice were infected i.p. with 10^9 metacyclic promastigotes and after 6 wpi were orally treated with MTF40 for 5 consecutive days. Animals were imaged before treatment (6wpi) and 72 h after the end of treatment (7wpi). Some of the animals treated with miltefosine were later immunosuppressed with 200 mg/kg cyclophosphamide administered by i.p. injection every three days for three doses maximum and imaged 4 days after the last dose. At the last time point animals were sacrificed and the parasite load of the liver, spleen, and femur bone marrow was determined by qPCR.

B. Representative ventral view images of Balb/c mice after treatment with MTF40 alone or combined with cyclophosphamide (MTF + CPP). (Unt) represents the animals treated only with the drug vehicle (water). Mice were imaged before treatment (6wpi), 72 h after the end of MTF40 treatment (7wpi) and 4 days after the last dose of CPP. Images are representative of n = 3–5 individuals per experiment.

C. Quantification of whole ventral bioluminescence, expressed as total flux (photons/s), from the experiment. Each point represents means ± SD of n individuals. (Unt) group was imaged for quantification of luminescence background (grey dashed line). Statistical significance calculated by one-way ANOVA: (*P < 0.05; **P < 0.01; ***P < 0.001).

D. *Ex vivo* images of mice organs after treatment with MTF40 or MTF10 for 5 consecutive days. Untreated mice (Unt), Lung (Lu), Liver (Li), Spleen (S), Heart (H), Kidney (K), Thymus (T) and Intestine (I).

E. Parasite burdens estimated by qPCR in untreated (Unt) and MTF40 or MTF10 for 5 consecutive days on liver, spleen, bone marrow and thymus. Each point represents means ± SD of n animals. Statistical significance calculated by one-way ANOVA: (*P < 0.05; **P < 0.01; ***P < 0.001).

Figure 7. Correlation between both *ex vivo* (top) and *in vivo* (bottom) bioluminescence values and parasite burdens in liver spleen and thymus. Bioluminescence was measured in vivo and ex vivo in ROIs around the corresponding organs and parasite loads were quantified by q-PCR after animals were sacrificed.

Figure S1. Localizations of the patches of black modelling clay in a mouse, whose ventral region was previously cream-depilated in order to prevent the interference of the more brilliant light source over the less potent areas.

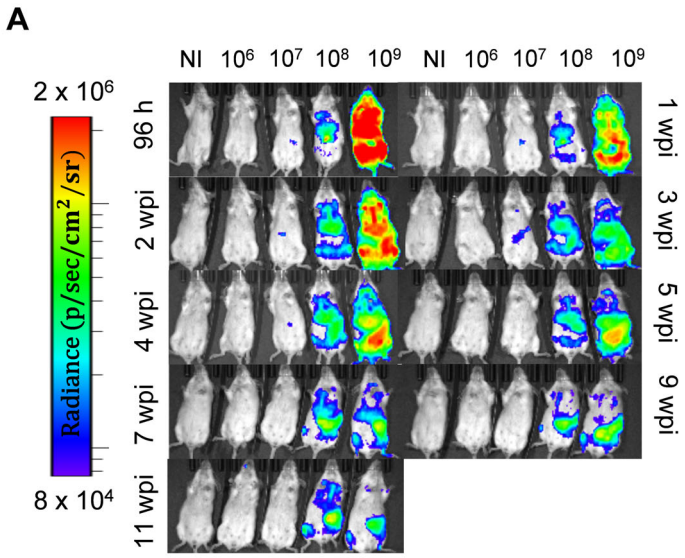
A
NI
10^6
10^7
10^8
10^9
NI
10^6
10^7
10^8
10^9
2 x 10^6
Radiance (p/sec/cm^2/sr)
8 x 10^4
96 h
2 wpi
4 wpi
7 wpi
11 wpi
1 wpi
3 wpi
5 wpi
9 wpi

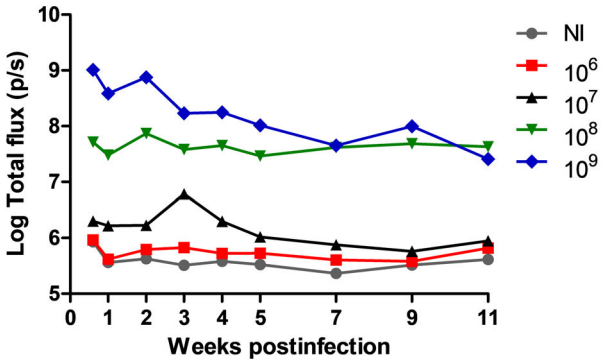
B
Log Total flux (p/s)
10
9
8
7
6
5
0
1
2
3
4
5
7
9
11
Weeks postinfection
NI
10^6
10^7
10^8
10^9

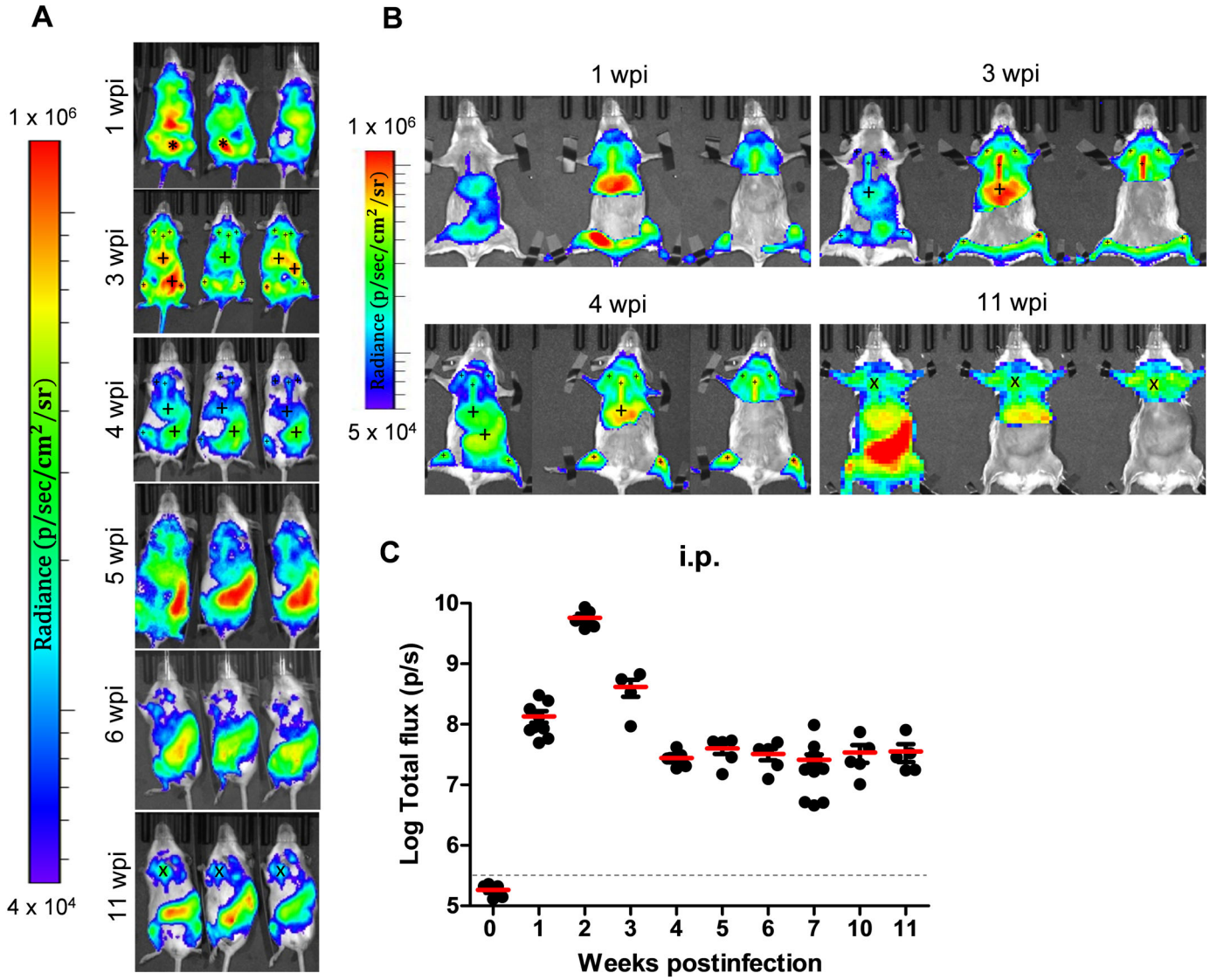
A
1 x 10⁶
Radiance (p/sec/cm²/sr)
4 x 10⁴
1 wpi
3 wpi
4 wpi
5 wpi
6 wpi
11 wpi
B
1 x 10⁶
Radiance (p/sec/cm²/sr)
5 x 10⁴
1 wpi
3 wpi
4 wpi
11 wpi
C
i.p.
Log Total flux (p/s)
Weeks postinfection

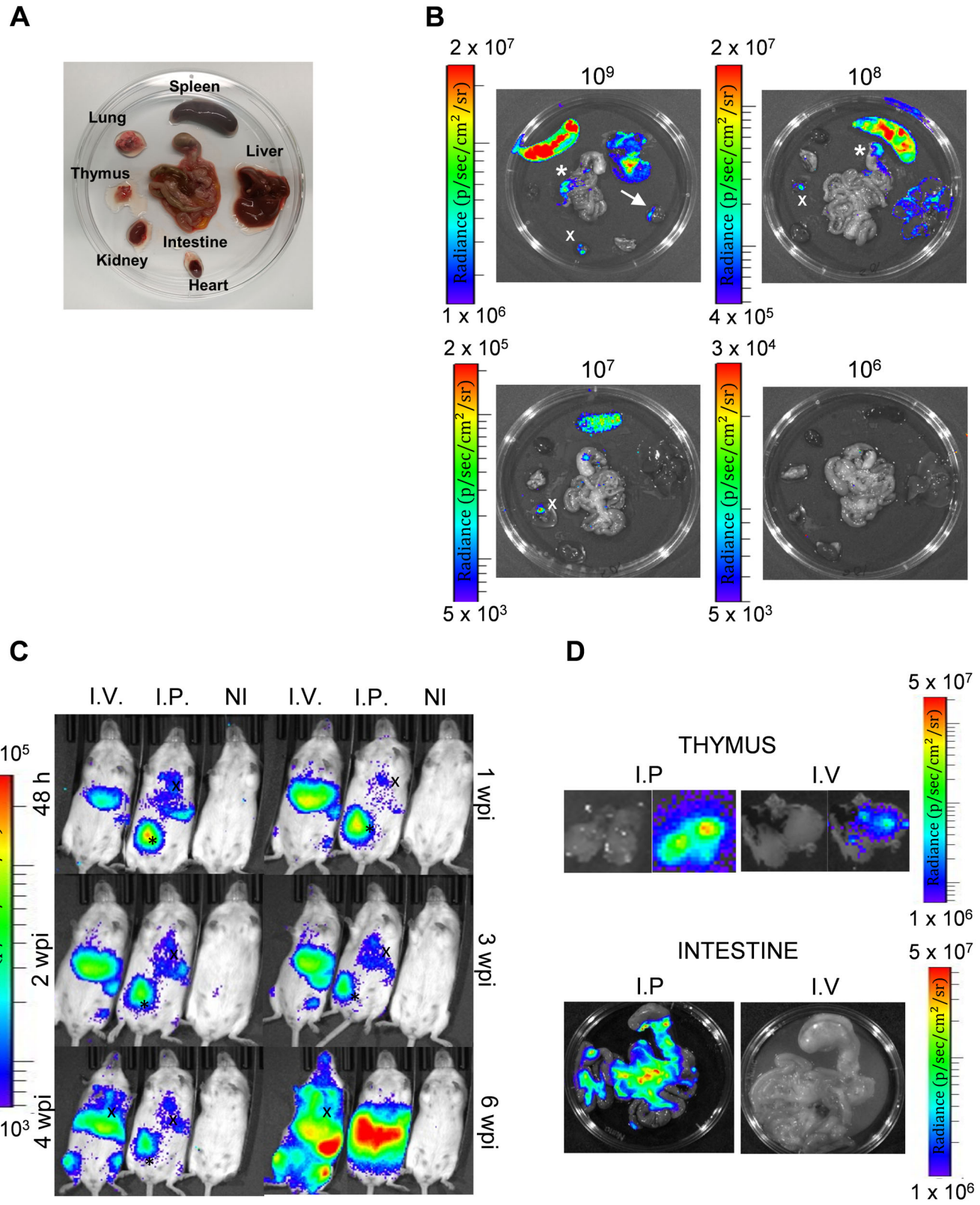
A
Spleen
Lung
Liver
Thymus
Intestine
Kidney
Heart
B
2 x 10^7
10^9
1 x 10^6
2 x 10^7
10^8
4 x 10^5
2 x 10^5
10^7
5 x 10^3
3 x 10^4
10^6
5 x 10^3
Radiance (p/sec/cm^2/sr)
C
I.V.
I.P.
NI
I.V.
I.P.
NI
3 x 10^5
6 x 10^3
Radiance (p/sec/cm^2/sr)
48 h
2 wpi
4 wpi
1 wpi
3 wpi
6 wpi
D
THYMUS
I.P
I.V
INTESTINE
I.P
I.V
5 x 10^7
1 x 10^6
5 x 10^7
1 x 10^6
Radiance (p/sec/cm^2/sr)

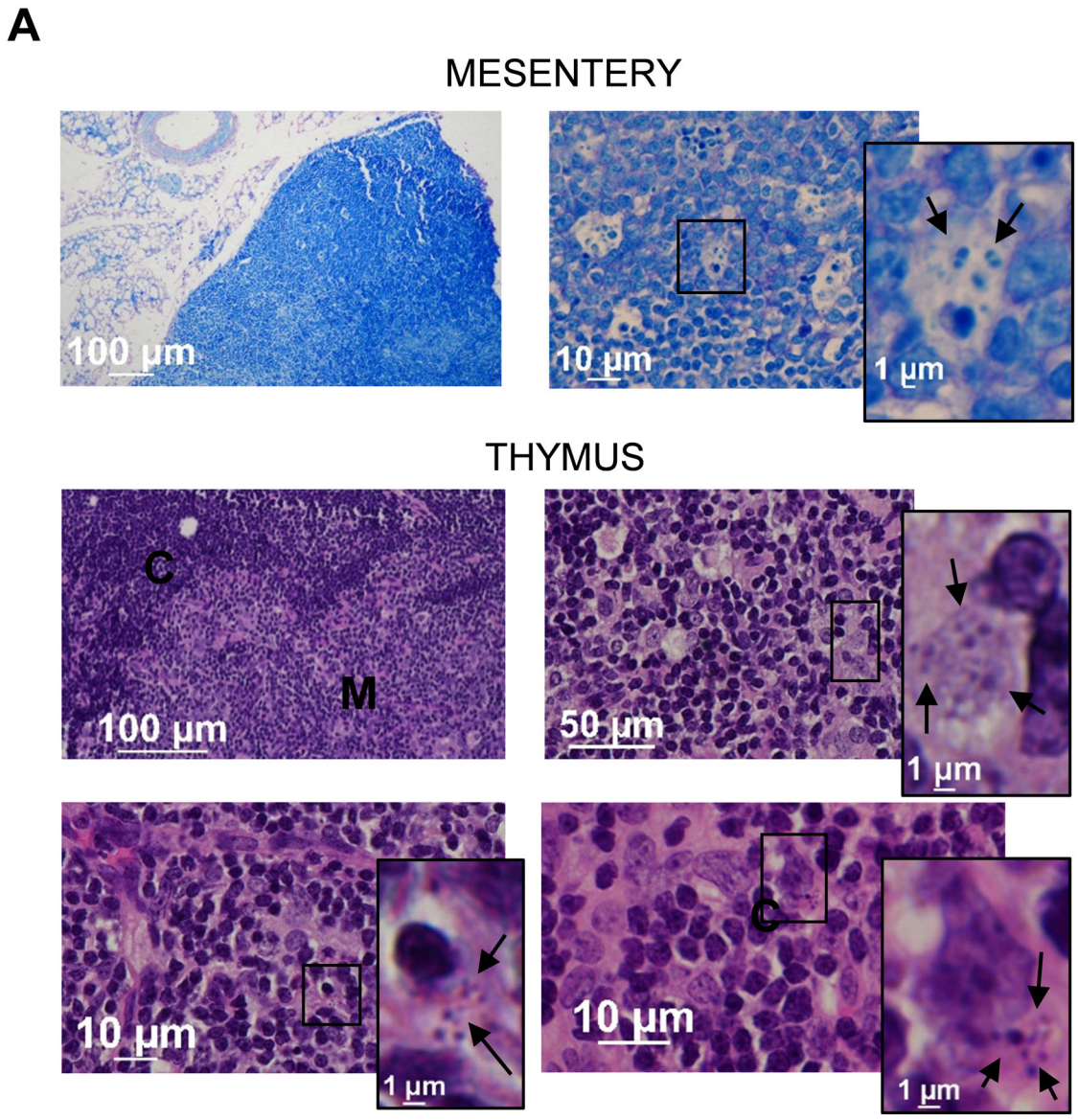
A
MESENTERY
100 µm
10 µm
1 µm
THYMUS
C
M
100 µm
50 µm
1 µm
10 µm
1 µm
C
10 µm
1 µm

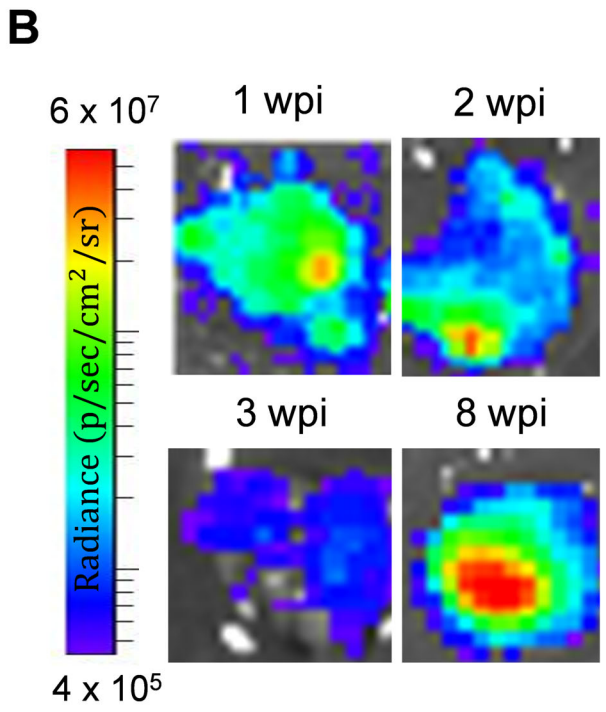
B
6 x 10⁷
1 wpi
2 wpi
Radiance (p/sec/cm²/sr)
3 wpi
8 wpi
4 x 10⁵

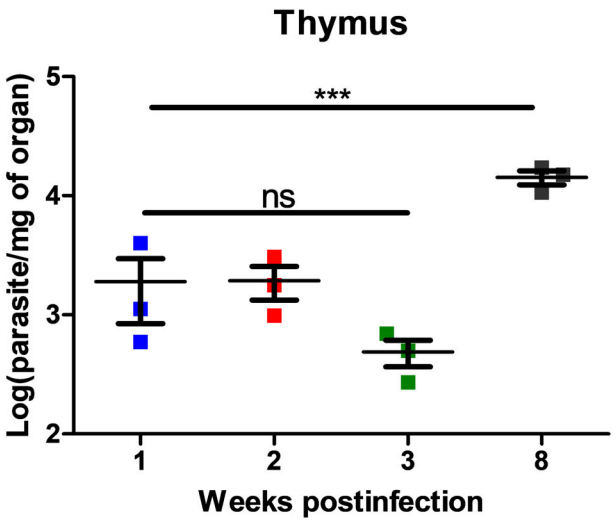
C
Thymus
***
ns
Log(parasite/mg of organ)
5
4
3
2
1
2
3
8
Weeks postinfection

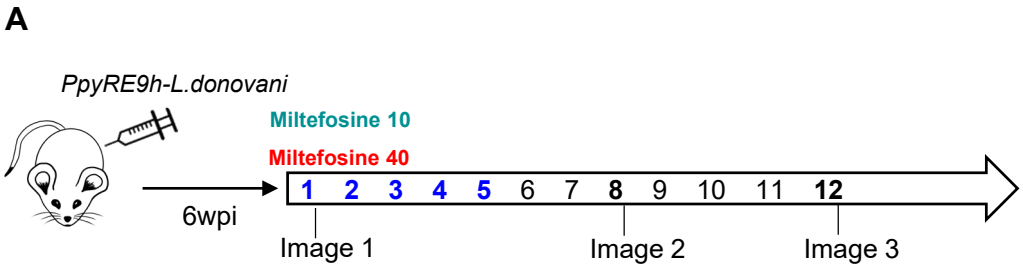
A
PpyRE9h-L.donovani
Miltefosine 10
Miltefosine 40
1 2 3 4 5 6 7 8 9 10 11 12
6wpi
Image 1
Image 2
Image 3

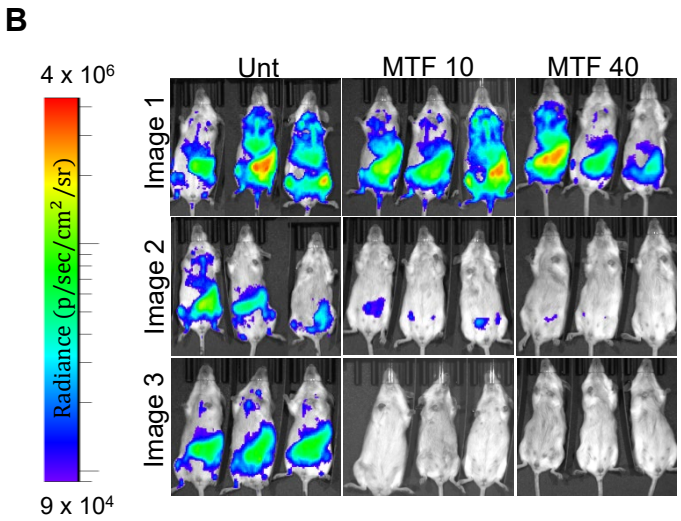
B
4 x 10^6
Radiance (p/sec/cm^2/sr)
9 x 10^4
Unt
MTF 10
MTF 40
Image 1
Image 2
Image 3

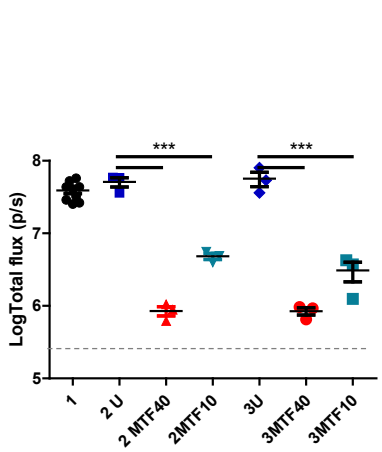
C
LogTotal flux (p/s)
***
***
1
2 U
2 MTF40
2MTF10
3U
3MTF40
3MTF10

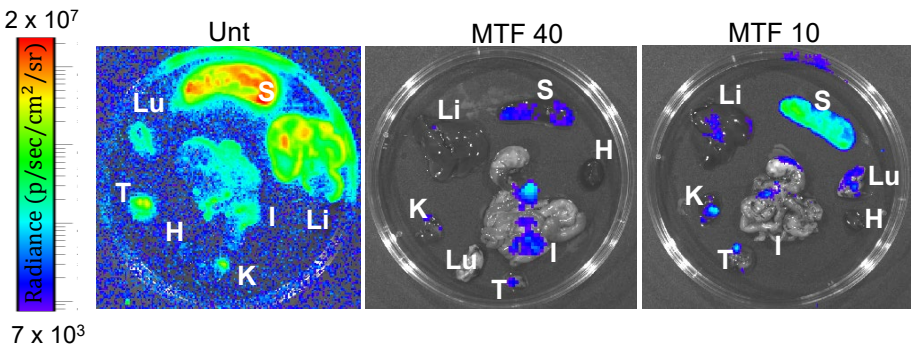
D
2 x 10^7
Radiance (p/sec/cm^2/sr)
7 x 10^3
Unt
MTF 40
MTF 10
Lu
S
T
H
I
Li
K
Li
S
H
K
Lu
I
T
Li
S
Lu
K
H
T
I

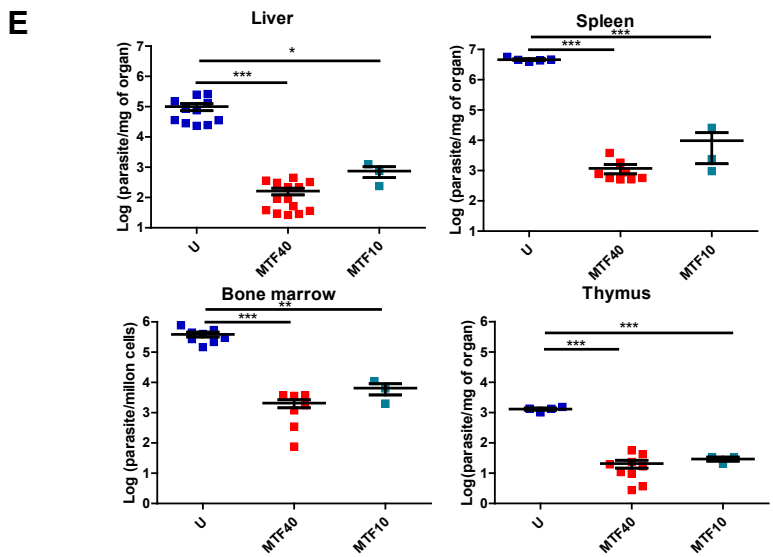
E
Liver
Spleen
Bone marrow
Thymus
Log (parasite/mg of organ)
Log (parasite/milion cells)
Log(parasite/mg of organ)
U
MTF40
MTF10

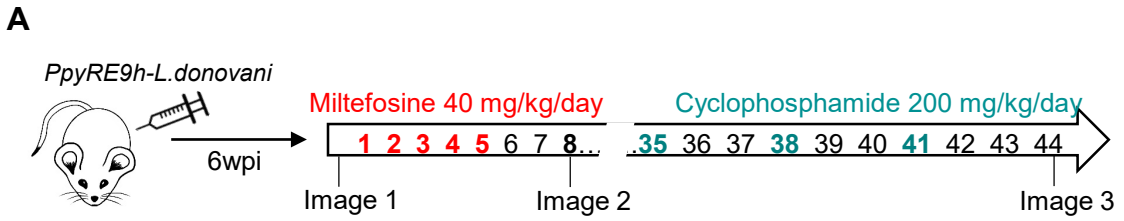
A
PpyRE9h-L.donovani
6wpi
Miltefosine 40 mg/kg/day
1 2 3 4 5 6 7 8...
Cyclophosphamide 200 mg/kg/day
.35 36 37 38 39 40 41 42 43 44
Image 1
Image 2
Image 3

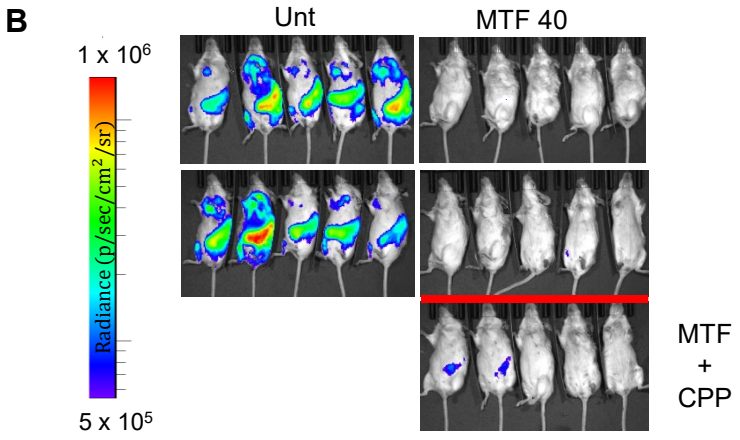
B
Unt
MTF 40
1 x 10^6
Radiance (p/sec/cm^2/sr)
5 x 10^5
MTF
+
CPP

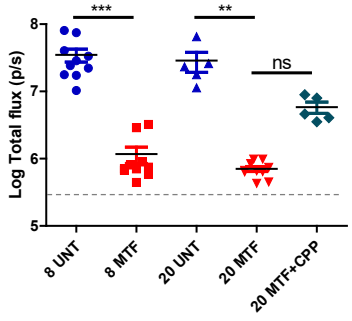
C
Log Total flux (p/s)
***
**
ns
8 UNT
8 MTF
20 UNT
20 MTF
20 MTF+CPP

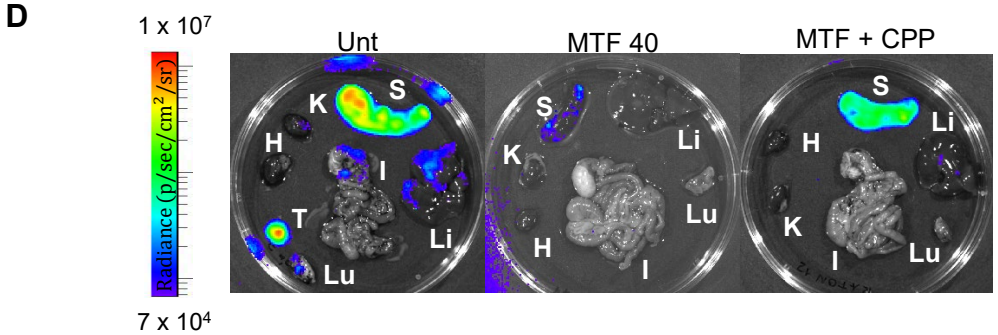
D
1 x 10^7
Radiance (p/sec/cm^2/sr)
7 x 10^4
Unt
MTF 40
MTF + CPP
K
S
H
I
T
Li
Lu

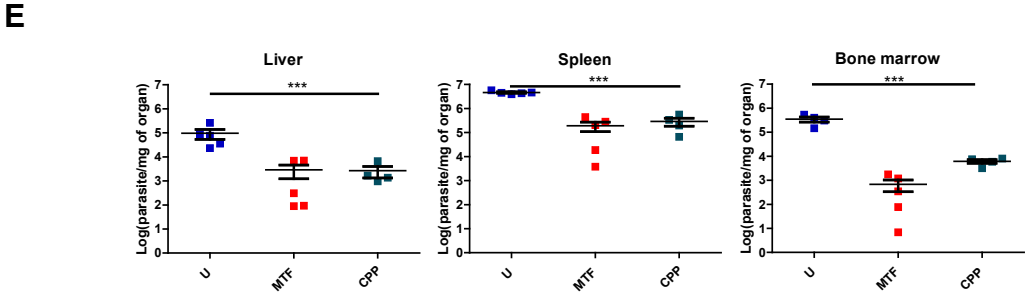
E
Liver
Spleen
Bone marrow
Log(parasite/mg of organ)
***
U
MTF
CPP

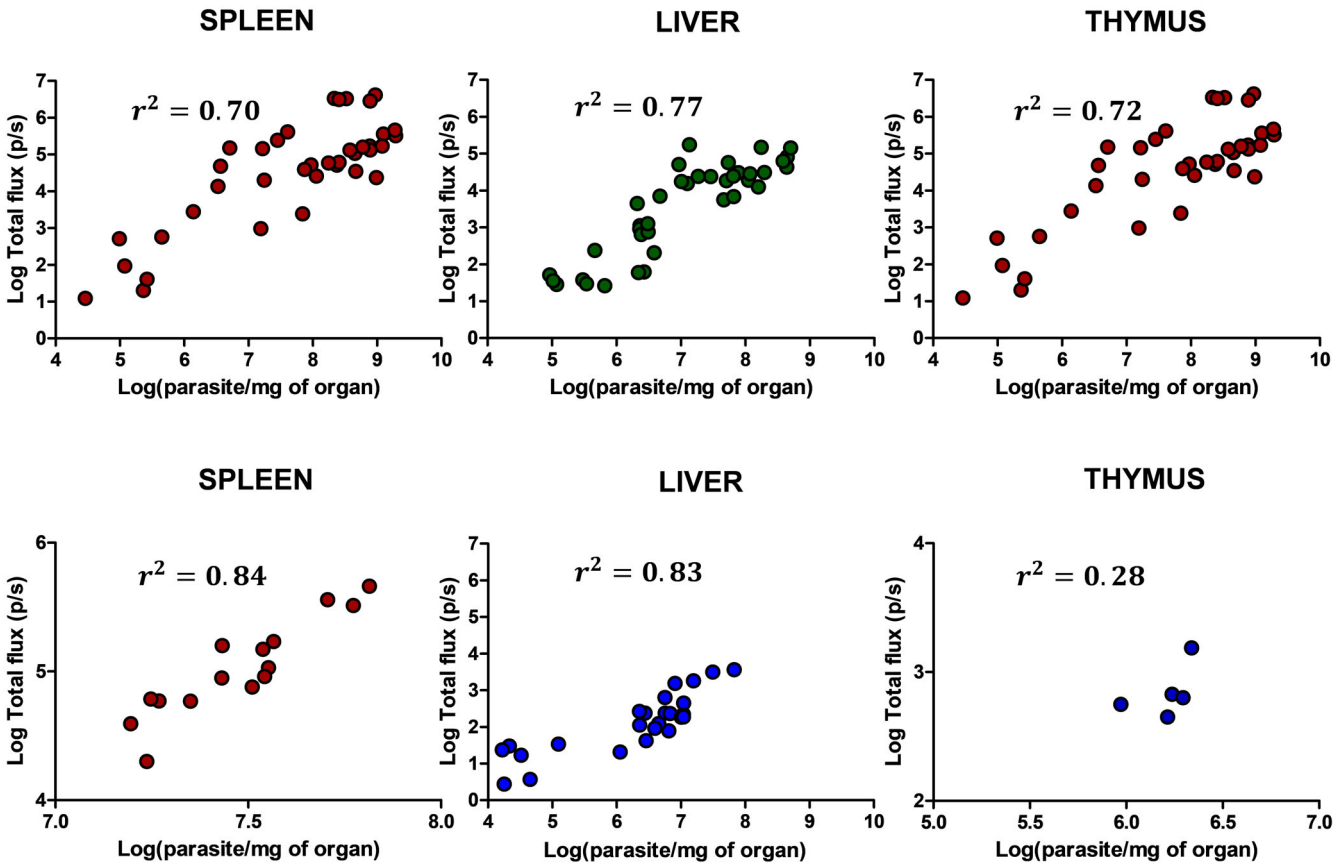
SPLEEN
$r^2 = 0.70$
Log Total flux (p/s)
Log(parasite/mg of organ)
LIVER
$r^2 = 0.77$
Log Total flux (p/s)
Log(parasite/mg of organ)
THYMUS
$r^2 = 0.72$
Log Total flux (p/s)
Log(parasite/mg of organ)
SPLEEN
$r^2 = 0.84$
Log Total flux (p/s)
Log(parasite/mg of organ)
LIVER
$r^2 = 0.83$
Log Total flux (p/s)
Log(parasite/mg of organ)
THYMUS
$r^2 = 0.28$
Log Total flux (p/s)
Log(parasite/mg of organ)